Physics of Plasmas

Electron–neutral collisions effects on Langmuir probe in the lower E-region ionosphere

Cite as: Phys. Plasmas **29**, 033511 (2022); https://doi.org/10.1063/5.0079761
Submitted: 24 November 2021 • Accepted: 02 March 2022 • Published Online: 21 March 2022

S. M. Brask, S. Marholm, F. Di Mare, et al.

Physics of Plasmas ARTICLE scitation.org/journal/php

Electron–neutral collisions effects on Langmuir probe in the lower E-region ionosphere

Cite as: Phys. Plasmas **29**, 033511 (2022); doi: 10.1063/5.0079761
Submitted: 24 November 2021 · Accepted: 2 March 2022 ·
Published Online: 21 March 2022

View Online Export Citation CrossMark

S. M. Brask,[1,a)] S. Marholm,[1] F. Di Mare,[1] S. Adhikari,[1] A. Spicher,[2] T. Takahashi,[3] and W. J. Miloch[1,b)]

AFFILIATIONS

[1]Department of Physics, University of Oslo, P.O. Box 1048, Blindern, 0316 Oslo, Norway
[2]Department of Physics and Technology, University of Tromsø, P.O. Box 6050, Langnes, 9037 Tromsø, Norway
[3]National Institute of Maritime, Port, and Aviation Technology, 6-38-1, Shinkawa, Mitaka-shi, Tokyo 181-0004, Japan

[a)]**Author to whom correspondence should be addressed:** s.m.brask@fys.uio.no
[b)]**Electronic mail:** w.j.miloch@fys.uio.no

ABSTRACT

We present the first set of particle-in-cell simulations including Monte Carlo collisions between charged and neutral particles used to simulate a cylindrical Langmuir probe in the electron saturation regime with a collisional electron sheath. We use a setup focused on the E-region ionosphere; however, the results of these simulations are analyzed in a general sense using dimensionless values. We find that the electron currents get enhanced as the collision frequency for electrons increases and the values of $\lambda_e/\lambda_D \to 1$, where λ_e is the electron mean free path and λ_D is the electron Debye length. In addition, we apply the simulation results to a sounding rocket experiment and show how we can correct the currents for the Investigation of Cusp Irregularities-4 sounding rocket due to collisions while it flies through the E-region.

I. INTRODUCTION

Langmuir probes have a long history and widespread usage in space measurements. The probes are usually designed with either spherical or cylindrical geometries, and they may have different setups for single- or multi-probe measurements. For example, the Rosetta spacecraft[1] had a two-probe setup designed for low-density measurements. This concept was inherited from earlier missions, like the Freja F4[2] and Cluster[3] missions, targeting relatively high density plasma in the ionosphere and magnetosphere. Another modern Langmuir probe system is the multi-needle Langmuir probe (m-NLP) used on the Investigation of Cusp Irregularities (ICI) rockets,[4–6] and NorSat-1.[7] The different setups require different theoretical equations to extract plasma parameters like temperature, density, and electric potential from the surrounding plasma. Usually, these theories are based on orbital limited (OML) theory,[8] which, in the electron saturation region, predicts that the current I_p to a probe p is given by

$$I_p = I_{th} K \left(1 + \frac{q(V_p + V_f)}{k_B T_e}\right)^{\beta}, \tag{1}$$

where k_B is the Boltzmann constant, q the elementary charge, and T_e the electron temperature. K and β are dependent on the probe shape. In particular, $K = 2/\sqrt{\pi}$ and $\beta = 0.5$ for ideal infinite length cylindrical probes and $K = \beta = 1$ for spherical probes. V_p and V_f are the probe potential and spacecraft body floating potential, respectively. $I_{th} = n_e q S \sqrt{\frac{k_B T_e}{2\pi m_e}}$ is the thermal electron current, where n_e and m_e are the electron density and mass with S being the surface area of the probe.

For the m-NLP system, ideally, we can eliminate some of the free parameters in Eq. (1) by taking the difference of the square of two m-NLP probes[4] to obtain an expression for the electron current that does not depend on the electron temperature. We could also take the current ratio to eliminate some parameters, and get an equation that is independent of the electron density. In any case, the direct measurement is an electric current to the probe, where for analysis ideal conditions are assumed, and one of these conditions is that the plasma is collisionless.

Most, if not all, scientific missions in space where Langmuir probes are used for measurements assume collisionless plasma conditions.[1,9] For the most part, this assumption is likely valid. However, in the lower E-region of the ionosphere—at ∼90–150 km—the collision frequencies between charged and neutral species are too high to call plasma in this region collisionless.[10,11] Several missions, like the

SPIDER missions[9] or the proposed orbital low flyer Daedalus,[12] have their focus on regimes with higher collision frequencies, where collisions are likely to impact the measurements in some way. In these cases, collisionless theories for the current collection of Langmuir probes must still be used since there is no collisional theory available. It is therefore assumed that the impact of collisions is small. However, this assumption is not trivial; there does not exist, to the best of our knowledge, any good source that would justify it, or would give a quantifiable method of correcting the currents collected by the Langmuir probes in collisional plasma. Interest in the complex and turbulent nature of the lower E-region is growing, due to radio echoes, signal degradation, and GPS scintillation.[13] In addition, there are several unanswered fundamental questions of plasma and atmospheric physics that are linked to this region.[14–16]

There have been some previous works on collisional effects on the currents collected by Langmuir probes.[17,18] While these articles focus on the ion collection (the negative probe potential) regime, discussions of the physical processes are applicable also for electron–neutral collisions. In Ref. 17, the authors report an increased ion current in the low-pressure (low-collision frequency) limit; this is attributed to the destruction of ion orbits around the probe. In addition, in the highly collisional case the ion currents are lower, limited by diffusion and drift to the probe. This is similar to the empirical results in Ref. 18 where they also report a peak in the ion current in the OML range when $\lambda_i \sim$ the sheath thickness. In their results, the value of λ_D/λ_i where this peak occurs ranges from ~0.2 to 0.5, meaning, there is a peak when λ_i is slightly longer than λ_D. However, some fundamental differences between electrons and ions means there will likely be significant differences between the charge–neutral collision effects on an ion or electron Langmuir probe current. One major difference is that for ion–neutral collisions, electrons usually act as a neutralizing/restoring background; this will not necessarily be the case for electron neutral-collisions.

Here, we will, for the first time, focus on the effects of electron–neutral collisions in the positive probe potential regime. The effects of ion collisions are in a sense more relevant than that of electron collisions because the mean free path is usually shorter for ions, giving it a wider range of applicability. However, experiments can easily be designed to circumvent the ion collisional effect by using probes that collect electron currents in the electron current regime where ion collisions can be neglected. This is where the need for an analysis of the electron collision effects arises. One possible reason explaining why this has not been done before is that simulating electron collisions is computationally more expensive, since we cannot treat the electrons as a fluid, as it is done in the studies of ion–neutral collision effects. We will here present the first fully 3D, kinetic simulations, of both electrons and ions, of a cylindrical Langmuir probe in the electron saturation regime, with a collisional electron sheath.

In this article, we will address both of the aforementioned issues using particle-in-cell (PIC) simulations. It is our intention that this article can be used as a reference to emphasize where the collisionless assumption holds. In addition, we will apply a method for building a function to correct collisional effects on the collected currents to a cylindrical Langmuir probe. We apply this method to the ICI-4 sounding rocket data to show an example of the effects of electron–neutral collisions through the whole E-region.

II. THE PIC SIMULATOR

This section reviews some important aspects of the new fully parallel 3D particle-in-cell (PIC) code PINC used in this study. There are three main classes of simulators employed for simulating plasma: PIC, fluid, and hybrid. A PIC simulator is well suited for studying kinetic effects and uses less assumptions as opposed to fluid or hybrid simulators. In particular, a fluid simulator solves the magnetohydrodynamic (MHD) equations, which assumes a Maxwellian form on the particle distribution. In hybrid simulators, a fluid treatment is usually performed on the electrons, and a PIC treatment is used for the ions. In a PIC simulator, we effectively solve the Vlasov equation using the method of characteristics, making no assumption on the particle distribution.[19] In collisional plasma, we have no a priori knowledge of the particle distributions; thus, a fluid or hybrid simulator is not well suited for this task. In addition, a fourth kind of simulator has emerged in recent years called Vlasov simulators.[20] Vlasov simulators solve the Vlasov equation directly and thus include kinetic effects. However, the collisionless assumption is usually included in the design of the simulator and would need further development to include charge–neutral particle collisions. The need for a new code lies in the fact that most codes that see widespread usage make some assumption—like treating electrons as a fluid—or are only capable to 2D simulations. There do exist some modern codes that do most of what we need, with the exception of for example charge–neutral collisions, which we could have modified for our use. However, by developing our own code we gain a larger degree of control in the implementation.

A. Applied algorithms

PINC uses the standard PIC main cycle[19,21,22] with the addition of object–plasma calculations using the conductive surface capacitance-matrix method[22,23] and charge-neutral collisions using the null-collision Monte Carlo collision (MCC) scheme.[21,24] Since particles exist in the space between grid nodes, on which the fields are defined, we need to translate between the particle positions and grid nodes. The interpolation between particles and field quantities on the grid is done with a first order weighting function, often referred to as Cloud-In-Cell (CIC). For each particle, its charge is weighted to the nearest grid nodes that define the cell in which that particle resides. This is done with a weighting function,[25] which weighs the particle by one minus its normalized distance to each of the nodes. Similarly, later the field quantities are superimposed at the particle position from each of the nodes by the same weighting function. We also use the so-called superparticles, meaning that each particle is to be considered a part of phase-space with a size in space equal to the grid cell volume, but a point in velocity. This gives the superparticles the ability to be rescaled to include several real particles and still allow for solving the same Vlasov equation.[19]

In PINC, we are interested in the electrostatic solution, neglecting any change in the magnetic field. However, a static magnetic field can still be included using the Boris algorithm.[26]

On the edge of the total simulated domain, we have chosen to use Dirichlet-type boundaries. We set the electric potential to be zero on the outermost nodes of the simulated domain and inject particles with a Maxwellian distribution.

The collision module is implemented using the null-collision MCC method described in Ref. 24, with the exception of a linear approximation to the collision frequencies, a method similar to the

one in Ref. 11. In order to maintain the correct collision frequency in the bulk plasma, in addition to adding the feature that slower moving particles collide less often than faster moving ones, we calculate the constant value of the cross sections that maintain this collision frequency. To do this, we begin with the probability for particle p to collide within a time step[24,25]

$$P_p = 1 - e^{-n_t(x)\sigma_T(\varepsilon)V_p(\varepsilon)}, \tag{2}$$

where n_t is the neutral density and V_p is the relative particle speed between the incident and target particle, with ε the particle energy. σ_T is the total collision cross section, which can be written as a sum of cross sections for each collision type i present. From this, we define an instantaneous collision frequency as follows:

$$\nu_{i,p} = n_t(x)\sigma_i(\varepsilon_p)V(\varepsilon_p), \tag{3}$$

where ν is the instantaneous collision frequency, at position x. In Eq. (3), the collision frequency $\nu_{i,p}$ can be considered as the instantaneous collision frequency of one particle, used to calculate that particle's probability to collide within a time step, using the neutral density at the particle and the particle's speed. If we average over the particle distribution using Eq. (3), and solve for the cross section, we get

$$\sigma_i = \frac{\bar{\nu}_i}{\bar{n}_t \bar{V}}, \tag{4}$$

where $\bar{n}_t$ is the constant average neutral density and $\bar{V}$ is the average speed of the particles, averaging over the particle distribution. We used here $\bar{\nu}_i$ to indicate that this is for the whole distribution, meaning that this is the actual collision frequency of the species. Although the cross sections σ_i are generally dependent on a single particle's energy, using the averages in this way now gives us a constant value at the average energy (temperature). Feeding this value back into Eq. (3) will also give an individual instantaneous collision frequency per particle but maintain the correct collision frequency when averaging over many particles. This gives us a model with a linear collision frequency in speed, i.e., $\nu \propto V$.

The collisional cross sections are complicated functions of energy in reality;[24] however, simplifications can be made by approximating the collision frequencies with a linear or squared function of the particle's speed.[11,27] We generally assume that the linear approximation is well justified for relatively low-energy plasmas such as those found in the vicinity of the Earth. Assumptions on the form of the collision frequencies are a topic of ongoing discussion, see Ref. 11, Sec. IV.

Usually, elastic electron–neutral collisions lead to a loss in energy for the electron due to the large difference in mass between the electron and neutral atom.[24] However, in some of the highly collisional cases presented in this article, this loss in energy, or lowering of temperature, could possibly increase the Debye length so much that the simulation becomes susceptible to the finite grid instability.[22,28] This is especially likely for the higher collisional cases (e.g., at least 6 and 7) because in cases 6 and 7 the particles will collide several hundreds of times before reaching the probe if they take the shortest path from the boundary. If this happened, it would be difficult to differentiate what part of the results were due to nonphysical numerical issues and what are actual physical results. We therefore use an energy conserving scheme, where we ensure that the energy before and after a collision is the same. This is done by storing the speed $|\vec{v}_p|$ of the electron p undergoing a collision before the scattering is performed. In previous works, calculation of the scattered velocity $\hat{v}_{scat}$ [see Ref. 24, Eq. (11)] is a unit vector, thus multiplying the particle speed before a collision with the scattered unit vector, i.e., $|\vec{v}_p| \cdot \hat{v}_{scat}$, will maintain the speed of the particle throughout the collision. Note that the collision frequency, i.e., probability to collide for a given particle is still energy (speed) dependent, so is the scattering angle.[24]

One important thing to note is that the MCC method includes an error in the number of particles to collide. In order for a particle to have a small probability of having two or more collisions, e.g., $r < 0.01$ in a single time step, the probability P_p of a collision in one time step should be $P_p < 0.095$.[24] This adds a constraint on the time step dt used for simulations, which will dominate for high collision frequencies.

B. Verification of simulation setup

During the development of PINC, many verification tests have been run; most of these are elaborate and outside the scope of this article, and we will here present some selected tests that are designed to cover the bigger picture. A detailed discussion of these tests can be found in the master's thesis of Killie,[29] Brask,[30] Holta,[31] and Nielsen.[32]

In order to verify the correctness and accuracy of PINC, we ran a set of verification tests. They can generally be split into two groups. The first set is for object–plasma interactions. The second set is for charge–neutral collisions. For object–plasma interactions, we first run a special case to compare to the OML theory. The case is essentially the same as in Ref. 23, and we use the same representation of a sphere with a radius of two cells. The actual geometry used is shown in Fig. 1. In addition to the floating potential, we compare the current collected by a biased Langmuir probe with the theoretical value. The current I_p in the electron saturation region is given by Eq. (1), where we have $V_f = 0$ since we are simulating a probe without the spacecraft.

In the test case, we used a mass ratio of $m_i/m_e = 100$, a density of $n_e = n_i = 1 \times 10^9 \mathrm{m}^{-3}$, and a temperature of $T_e = T_i = 1000$ K. For the floating potential test, we use a radius of $0.06\lambda_D$ in order to directly compare with Ref. 23. After running the simulation until it reaches a steady state, we get a floating potential of -0.1260 V, or $-1.46k_BT/e$, which is 3% of the theoretical value. When running the simulation again but with a bias of 2 V and again using a radius of 0.06 λ_D, we get a current of 4.310×10^{-8}A to the probe compared with the theoretical value given by Eq. (1), which is 4.102×10^{-8}A. This gives a percentage difference of 5%. The differences in values we obtain

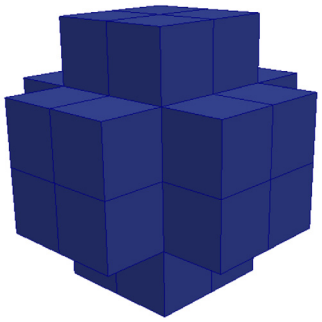

FIG. 1. Discretized geometry of a sphere used in the spherical OML test case.

from the simulator and theory might be explained by the ambiguity in the radius of the sphere. The sphere is approximated by numerical cells, which are in fact cubes.

An additional test was performed to verify the current collection. In this test, we use a slightly more complicated geometry for the probe, a cylinder which is longer than the Debye length and has a radius that is shorter than the Debye length. We then compare the collected current to an independent PIC code, PTetra.[33,34] PTetra differs from PINC in one major way in that it uses nonuniform grid spacing. For verification, we used the collisionless case detailed in Sec. III and ran the simulation with the exact same probe geometry in PTetra and PINC. We ran the simulation both with a probe bias of 4.5 and 7.5 V. The steady state currents from PINC and from PTetra are shown in Table I. In this comparison between PINC and PTetra, we did not expect an exact agreement due to significant implementation differences between PINC and PTetra. Still, we obtain a difference of ∼8%–9% in both cases, which we deem to be adequate for this case.

The most important test for verifying the correctness of the collisional module is that the number of colliding particles is consistent with the collision frequency. This is obtained from the probability for a particle to undergo a collision within a time step,[24,25] given by

$$P_p = 1 - e^{-\nu_p \Delta t}, \tag{5}$$

where P_p is the probability for particle p to collide in time Δt, with collision frequency ν_p from Eq. (3). The number of colliding particles in a simulation per time step will then on average be

$$N_c = N_T \bar{P}, \tag{6}$$

where $\bar{P}$ is the average probability, using the average collision frequency from Eq. (5). N_T is the total number of particles in the simulation. Note that with this definition, using probability, the number of colliding particles will change as the weighting of the superparticles changes, as it should. To verify that we collide the correct number of particles, we ran a simulation on an $8 \times 8 \times 8$ grid with 420 particles per cell. With a time step of $0.1\omega_{pe} = 1.77 \times 10^{-8}$ s and $\nu = 4 \times 10^5\ \mathrm{s}^{-1}$, we get $N_c = 758$ colliding particles per time step. The result was an average 769.7 collisions for electrons and 766.2 for ions. This test was run for a relatively short time, and we expect the numbers to get closer to N_c if we run the text longer; however, the largest error here is 1.5%, which is lower than other sources of error.

In addition to the collision frequency change, we checked that the change in energies and scattering angles due to a collision was consistent with the equations given in Ref. 24. In addition, to check that there was no systematic error in the scattering angles, we checked that the average of these was zero, i.e., angle has no preferred direction but is random.

TABLE I. Summary of parameters for the current collection test where we compare PINC to PTetra.

	PINC	PTetra
4.5 V	-4.59×10^{-6}A	-5.05×10^{-6}A
7.5 V	-6.95×10^{-6}A	-7.55×10^{-6}A

III. SIMULATION SETUP

In this section, we will go through the simulation setup used. The set consists of twelve simulations: six of them are run with a probe bias of 4.5 V and the other six are run with a probe bias of 7.5 V. We maintain the plasma parameters fixed with the exception of collision frequency, such that we isolate the effects of collisions on the two different biased probes. The parameters are based on EISCAT Svalbard Radar (ESR) data collected at 120 km altitude on 19 February 2015, at 22:00, at the launch of the ICI-4 sounding rocket, and are listed in the first panel in Table II. The values provided correspond to the mean quantities obtained from ESR UHF between 22:05:59 and 22:15:59 UT using 120 s integration time.

ICI-4 was launched from Andøya, Norway, in the nightside aurora and was in total darkness during the entire flight. The collision frequencies for both ions and electrons vary in power from 0 to 7. ICI-4 had four Langmuir probes biased at 3, 4.5, 6, and 7.5 V. Ideally, we would want to simulate all four probes; however, since we are somewhat limited by available computational resources we pick the 4.5 and 7.5 V probes. We are mostly interested in the electron collision frequencies as the collected currents are in the electron saturation region, and electron dynamics will be the dominating effect. In the E-region ionosphere, the dominant ion species are NO^+ and O^{2+}; however, in the simulations we use He^{4+}. It is a common trick in PIC simulations, however, to reduce the ion mass. This is because otherwise, the ion dynamics gets so slow that they incur a high computational cost—by increasing the time steps needed—and, therefore, the computational time needed to reach steady state. Reducing the ion mass will in turn increase the ion current. However, in the electron saturation region, the ion current is nonetheless negligible compared to the electron

TABLE II. Input parameters to the PIC simulator. The simulation parameters are based on observational data from ESR and NRLMSISE-00 Model 2001. The plasma parameters come from ESR and neutral densities and temperatures used for calculating collision frequencies come from NRLMSISE. The simulation ID is assigned from the power of the electron collision frequency ν_e.

Parameters	Value	
dx, dy, dz (m)	0.002	
dt (s)	5×10^{-10}	
Time steps	100 000	
Density (e, i) (m^{-3})	9.597×10^{10}	
T_e (K)	441	
T_i (K)	475	
m_e (kg)	9.109×10^{-31}	
m_i (kg)	6.646×10^{-27}	
Simulation ID	ν_i	ν_e
0	0	0
2	8.737×10^2	2.911×10^2
3	8.737×10^3	2.911×10^3
4	8.737×10^4	2.911×10^4
5	8.737×10^5	2.911×10^5
6	8.737×10^6	2.911×10^6
7	8.737×10^7	2.911×10^7

current. In addition, there is no collisional coupling between electrons and ions. The reduced mass therefore should not affect our results.

For comparison, we chose a probe geometry that mimics the probes from ICI-4. The exact geometry can make a difference, and we are simulating a probe with length $\sim 5\lambda_D$ such that the probe current likely is impacted by the finite length effect[35] and the fact that the probe is actually mounted on a guard, not included in the simulations. In the following analysis, we assume that such effects do not depend on the collision frequency such that when we take the ratio of two currents, effects like the finite length effect will disappear. Due to the uniform grid employed in PINC, our simulated "cylindrical" probe is actually a rectangular box with size $1 \times 1 \times 12$ cells, that is $0.002 \times 0.002 \times 0.024\,\mathrm{m}^3$. We also use a simulated domain of $128 \times 128 \times 128$ cells, which is $0.256 \times 0.256 \times 0.256\,\mathrm{m}^3$. That gives each side of the domain a length of 54.8 Debye lengths.

In Table III, we have listed some derived parameters for the simulations, in particular the dimensionless parameter mean free path (λ_e)/Debye length (λ_D). To calculate λ_e, we use the definition

$$\lambda_e \equiv \frac{\text{particle speed}}{\text{e} - \text{n collision frequency}} = \frac{v_{th,e}}{\nu_e}. \tag{7}$$

Here, $v_{th,e}$ is the electron thermal speed and ν_e is the electron–neutral collision frequency. In the remainder of this article, it is therefore understood that when we talk about the mean free path it is the electron mean free path λ_e.

The usual assumption on collisionless conditions is stated as $\omega_{pe}/\nu_e \gg 1$, where ω_{pe} is the electron plasma frequency. This inequality leads to the equation

$$\frac{\lambda_e}{\lambda_D} = \frac{v_{th,e}/\nu_e}{v_{th,e}/\omega_{pe}} = \frac{\omega_{pe}}{\nu_e} \gg 1. \tag{8}$$

So, both the dimensionless parameters, λ_e/λ_D and ω_{pe}/ν_e, can be used interchangeably; but we will use the parameter λ_e/λ_D as a measure of the collisionality in plasma.

In order to calculate the collision frequencies between the plasma particles and neutral particles, we used the equations given in Ref. 36 and the data for neutral temperatures and densities from NRLMSISE-00 Model 2001.[37,38] The NRLMSISE model is an empirical model based on several sources of data, used to calculate the neutral density and temperature in Earth's atmosphere. NRL stands for the US Naval Research Laboratory. MSIS stands for mass spectrometer and incoherent scatter radar, which was the source of data in the original form of the model. Later versions also include satellite drag data. The last E stands for exosphere, indicating that the model extends through the whole exosphere of the Earth.

TABLE III. Derived parameters for Table II.

Parameters	Value
ω_{pe} (rad/s)	1.75×10^7
λ_{de} (m)	0.004 678
λ_{e0}/λ_D	∞
λ_{e2}/λ_D	60 038
λ_{e3}/λ_D	6003.8
λ_{e4}/λ_D	600.38
λ_{e5}/λ_D	60.038
λ_{e6}/λ_D	6.0038
λ_{e7}/λ_D	0.6004

IV. RESULTS

The results of the simulations are divided into three subsections. First, we provide general results of the current collected at two different bias values of the Langmuir probe, where the only varied parameter is λ_e/λ_D. Second, we carry out an additional test to study the dependence of the current on the plasma parameters at a fixed value of λ_e/λ_D. Third, we quantify the simulation results with a least squares regression to a well-behaved function.

A. Simulation results

In this section, we present results from the simulations described in Sec. III.

Figure 2 shows plots of the electron densities perpendicular to the probe and through the short side in the center of the probe. The vertical black dotted line represents the probe surface. In the figure, we added one plot from each simulation from the 4.5 V bias cases, such that each plot represents a collision frequency, or equivalently a value of λ_e/λ_D. We chose to omit including a figure for the 7.5 V case as it shows similar density profiles, only with the exception of higher peak density values.

As expected, when the collision frequencies increase, the peak electron density in the probe sheath gets lowered. However, there is one exception, from simulation 2 we see a small increase in the peak density. Noting that this increase is small enough to be within simulation error, it might indicate a higher trapping rate for the electrons, similar to the processes described in Refs. 17 and 18, but for electrons instead of ions. For relatively low collision frequencies, the electron-neutral collisions transfer radial momentum to angular momentum, trapping the electrons in orbit. This happens at a higher rate than the

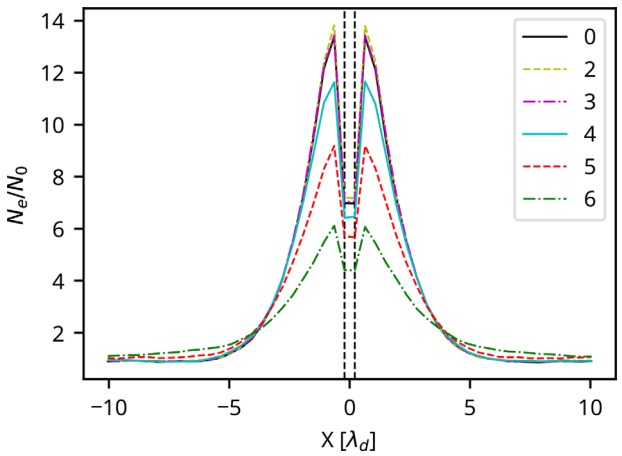

FIG. 2. Lineplots across the middle of the probe traversing the short side. The plot shows the electron densities. Density values are normalized by N_0, the ambient background density of the electrons, and length is given in Debye lengths. Densities are averaged over the last 1000 time steps. The plot shows only the contribution from particles, omitting the contribution from surface charges on the probe.

opposite effect, where the colliding electron orbits are destroyed and the electrons fall toward the probe. For the rest of the simulations, the latter effect seems to be dominating, the high rate of electrons getting pushed out of orbit is effectively lowering the density close to the probe. The presheath, at $\sim\pm 5$–$10\lambda_D$ has the opposite behavior, with lower values for lower collision frequencies, and higher densities as the collision frequencies rise.

The development of the currents to the probe in time is presented in Fig. 3. Comparing the 4.5 V (a) cases to the 7.5 V (b) cases, we see that the overall behavior between these is the same. For the cases up to case 6, that is, for all cases where $\lambda_e/\lambda_D > 1$, the currents stabilize at higher values as the collision frequencies rise and λ_e gets lower. The development of the transient in the current slows down and stabilizes at an enhanced value, compared to the collisionless case. The reason for higher current values is the same as that for the lower densities seen in Fig. 2—as the collision frequency rises, more particles are knocked out of orbit and get collected by the probe.

The impact of varying the electron-neutral collision frequency on the collected current can be seen in Fig. 4. In Fig. 4(a), the currents are normalized, with I_0 being the zero collision frequency (collisionless) current obtained from simulations. The black dotted line indicates a 10% change with respect to the collisionless case. The current ratio, see Fig. 4(b), is the ratio of the currents at a bias value of 7.5 V to the 4.5 V simulations at different values of λ_e/λ_D.

The importance of current ratios is to visualize the difference in the impact of collisions for the two different probes. If the variation in collision frequency impacts probes at different potentials equally, the

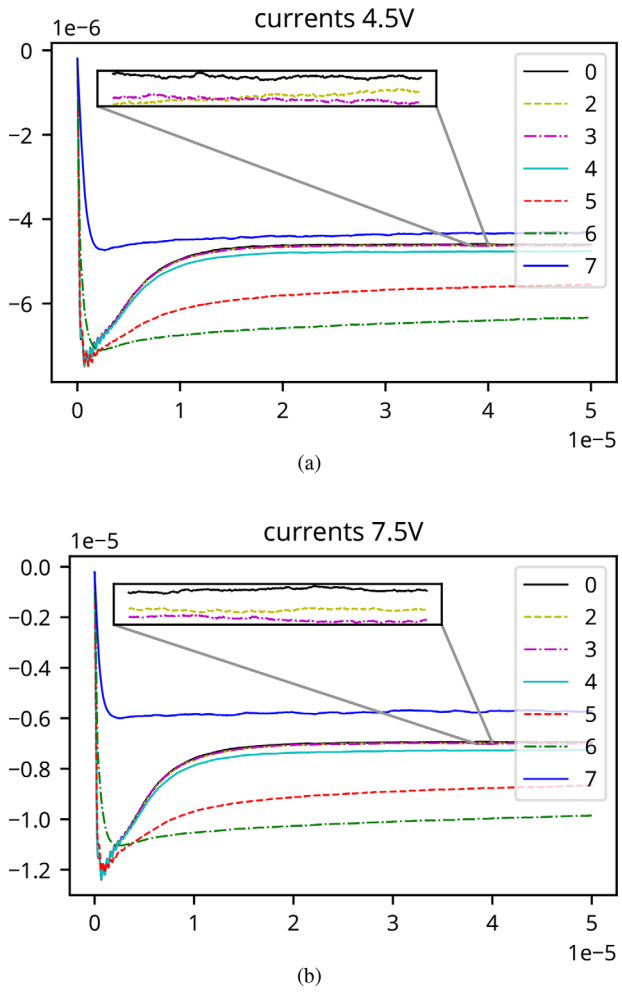

FIG. 3. Development of the currents to the simulated probe at 4.5 V cases (a) and 7.5 V cases (b). The numbers 7, 6, 5, 4, 3, 2, and 0 refer to the order of magnitude of the electron collision frequency. Values are given in SI units. Both plots include a 10× zoomed-in area to show the differences in cases 0, 2, and 3. In order to remove noise, an exponential moving average filter using a relaxation time of ten time steps was applied. (Associated dataset available at https://doi.org/10.5281/zenodo.5906749) (Ref. 39).

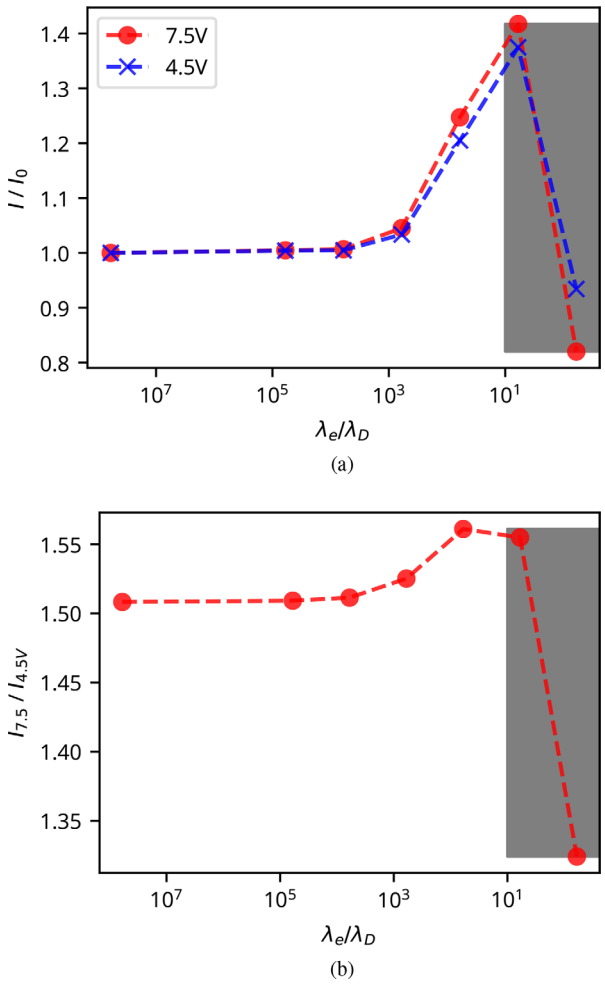

FIG. 4. Comparison of single currents (a) and current ratios (b) for case with fixed plasma parameters, but with varying collision frequency. Currents are collected at two different positive bias values: 4.5 and 7.5 V. All values are averaged over the last 500 time steps. The gray area shows where the mean free path has the same order of magnitude as the Debye length. The zero collision, infinitely long mean free path case 0 is represented by the number 6×10^7. (Associated dataset available at https://doi.org/10.5281/zenodo.5906749) (Ref. 39).

plotted line in Fig. 4(b) should be straight. Taking the ratio of two probes a and b using Eq. (1), we get

$$I_a/I_b = \frac{\left(1+\frac{q(V_a+V_f)}{k_B T_e}\right)^{\beta}}{\left(1+\frac{q(V_b+V_f)}{k_B T_e}\right)^{\beta}}, \tag{9}$$

which is independent of density and constant for constant values of floating potential V_f, electron temperature T_e, and probe geometry β. In these simulations, we control V_f and T_e, and maintain them as constants, so the changes must be explained either with β which is possible since the probe has a finite length[35] or as a purely collisional effect.

In both plots in Fig. 4, the x axis is log scaled using a base 10 logarithm. From the normalized currents, we see that the currents increase with increasing collision frequency (lower λ_e) for cases where $\lambda_e/\lambda_D > 1$. In addition, the curve seems to follow an exponential increase, at least for the first five points. This exponential increase suggests that the change in currents linearly depends on λ_e/λ_D due to the log scaled x axis. We will test this dependency in Secs. IV B and IV C. For the current ratios, we observe a similar increase—suggesting that the collisions impact the two different bias values differently. However, the percentagewise change is small and might therefore be negligible for the present setup. We do not know if this change will be larger for other setups. It might also impact some analysis methods to a larger degree, if one takes for example the difference of the squared currents. In any case, we will include most of these differences in the correction later.

For the case 7 current value, it is likely true that it will be lower than at least the case 6 currents, based on the observations from Fig. 3. Currently, we do not know if this value can be trusted, as it is likely that when $\lambda_e/\lambda_D < 1$ the plasma dynamics are no longer dominated by electromagnetic forces. Although this in itself should not invalidate the simulations, this point should be analyzed with care. In addition, we highlighted the area where the mean free path has the same order of magnitude as the Debye length in gray as an area of concern, which needs additional analysis and verification in the future. However, the trend makes physical sense as electrical resistance will dominate at these higher collision frequencies. It is also consistent with a similar process for ions.[18] The point is added for consistency with the previous plots, and future reference.

B. Dependence on plasma parameters with fixed λ_e/λ_D

As we saw in Fig. 4, there is a dependence of the collected current on the parameter λ_e/λ_D. However, it might seem unclear if there are additional dependencies on plasma parameters. In order to answer this question, we set up an additional test. We modify two additional simulated parameters, starting with the setup in Table II; for the first additional case, we increase the temperature by an order of magnitude, and for the second we increase the temperature by a factor of 10 and the density by a factor of 5. In each case, we maintain the parameter $\lambda_e/\lambda_D = 60$ by varying the electron collision frequency. In addition, we rescale the simulation grid to maintain the probe size with respect to λ_D. The idea is that if we change the plasma parameters, but maintain all the dimensionless parameters at constant values, if there is no dependence on other parameters, we should get the same value in each case for I/I_0, the ratio of collisionless current to the collisional current. To this end, we also need to rescale the probe bias. To do this, we use the dimensionless potential

$$\eta = \frac{qV_p}{k_B T_e}. \tag{10}$$

In this case, we get a value of $\eta \simeq 118$; for both of the new cases to maintain a constant η, we need to increase the bias by an order of magnitude since the temperature increases by an order.

From Table IV, we see that the value of I/I_0 can be considered constant as the differences are small enough to be associated with the simulation errors, such as the finite grid, finite time step, and limited simulation box. For these values, the mean is 1.2216 with a small standard deviation of 0.0095; this small standard deviation supports the fact that normalized currents are dependent only on the dimensionless parameter λ_e/λ_D at a constant η. It is important to note that since η is temperature dependent, realistically, in a rocket mission as temperature and floating potential of the spacecraft changes, η will also change.

C. Quantifying the changes in currents

As mentioned previously, the currents in Fig. 3 seem to follow an exponential curve. We will in this subsection show how we can use these results from the simulations to fit a suitable exponential function to the data points. This function will then give a quantifiable method for correcting the collected currents, which could be used in post-processed/corrected L2 data products for sounding rocket missions or low flying orbiters.

There are several candidate functions we can fit to. We chose one that will be suited for the low to medium collisional range, as this will be usable for most cases in space plasmas. If we were to include higher collision frequencies, this function would need a more complex form. To this end, we use only the five lowest collision frequency points. The function we chose is of the form

$$I/I_0 = 1 + \gamma_{corr} = 1 + 10^{A+Bx}, \tag{11}$$

where I is the collected current and I_0 is the zero collision current. I_0 can be any successful theoretical or measured collisionless current; for example, we may use the OML value of the current for I_0, then I is the collisionally corrected OML current. γ_{corr} is a correctional term, in this case an exponential $\gamma_{corr} = 10^{A+Bx}$. The variable x is the ($\log_{10}$) value of λ_e/λ_D. γ_{corr} could have been the natural exponential, this would just change the coefficients A and B. We chose to use base 10 for consistency with the simulations and plots.

We perform a least squares regression where we minimize the residual sum of squares defined as $RSS = \sum_i (y_i - \tilde{y}_i)^2$. Here, y_i are the values from the simulations and $\tilde{y}_i$ are the values we get from Eq. (11) at the same values of $x = \log_{10}\lambda_e/\lambda_D$.

In order to evaluate the quality of the fit, we use the coefficient of determination called "R square" value, defined as $R^2 = 1 - RSS/TSS$,

TABLE IV. Normalized current values for three cases with different plasma parameters, but fixed λ_e/λ_D.

	Original	Added case 1	Added case 2
I/I_0	1.212	1.222	1.231

TABLE V. Table of coefficients, and their residual sum of squares from the fit of Eq. (11) to the simulation data.

	A	B	R^2
4.5 V	0.76	−0.81	0.999 81
7.5 V	0.72	−0.74	0.999 76

where $TSS = \sum_i (y_i - \bar{y})^2$ and is the total sum of squares. Generally, a higher value of R squared indicates that the fit is better, and if $R^2 = 1$ the model perfectly describes the data. As we see from the values of R^2 in Table V, the fit we obtain is good. Since the parameters are found using a setup applicable to the launch of the ICI-4 sounding rocket, using these in Eq. (11), this gives us a correction due to collisions that we can apply to the ICI-4 data for the 4.5 and 7.5 V probes. As mentioned above, the values obtained for the coefficients A and B are based on simulations using an energy-conserving scheme for the electron–neutral collisions. It should be noted that this assumption might be nontrivial, and the inclusion of energy-loss during the electron–neutral collisions will likely further enhance the collected current, which would change these coefficients to some degree.

Finally, we can apply this fitted function to the ICI-4 Langmuir probe data. In addition, we need λ_D and λ_e. The plasma temperature and density are again obtained using ESR data with a resolution of 5 km in the vertical direction and the neutrals' (N_2, O, and O_2) temperature and density are obtained with NRLMSISE-00 Model 2001,[37,38] and λ_e is calculated using collision frequencies from Ref. 36. From this, we get a value of λ_e/λ_D at each 5 km, values are interpolated between the 5 km resolution in Fig. 5(b). Note also that this calculated λ_D is not accurate within these 5 km; however, this should not make a large impact since it is the order of magnitude that is important.

The result of the collisional correction is shown in Fig. 5(a). Both the original uncorrected current $I4$ and the corrected $I4_0$ probe current are plotted. A bandpass filtering was performed on the uncorrected current to remove the spin from the payload and the first three harmonics. The bandpass filtering is then effectively also applied to the corrected current through the uncorrected current. In Fig. 5(b), the ratio of these is plotted in a similar manner as in Fig. 4. From the $I4/I4_0$ ratio, we see that the corrections are small above 120 km and negligible above 160 km. For ICI-4, if high accuracy in the currents is required, then it will be important to use collisional corrections on data up to ∼160 km, and under 120 km collisional corrections should always be used. It is reasonable to assume that similar heights will be of importance for other missions.

V. CONCLUSIONS AND FUTURE PERSPECTIVES

The results of the simulations indicate that the effect of electron–neutral collisions on an electric current collected by a cylindrical Langmuir probe, biased in the electron saturation regime, generally leads to an enhancement in the collected current when $\lambda_e/\lambda_D \to 1$. With the simulation results, we could fit a function to the simulation results for the probes biased at 4.5 and 7.5 V for plasma parameters relevant for ionospheric conditions. These two functions were consistent with the simulations at ionospheric altitudes down to 100 km, at which point additional simulations and a non-linear function for the exponent of γ_{corr} would be needed. This method of using simulations results for correcting experimental data is general, and it can be deployed on a per-mission basis. We expect that the values we obtained and used in Eq. (11) should hold for ionospheric conditions similar to the ICI-4 sounding rocket mission presented here. However, at present we feel that additional simulations should be run in other missions to verify or obtain new parameters. In addition, since the model presented here for ICI-4 is not verified outside of simulations, experimental verification should be done in the future.

It may be possible to extract plasma parameters omitting the collisional effects by taking, e.g., the ratio of two probes. If the collisions impact the probes at the same rate, the collisional effect should disappear. However, we see some evidence that this is not the case for higher collision frequencies in Fig. 4(b). More precisely, as long as the dependence on the dimensionless collision parameter λ_e/λ_D does not change with varying η, i.e., the term γ_{corr} in Eq. (11) appears to depend weakly on η. In the present study, the η dependence will be included in Eq. (11) as long as the linear assumption holds, which in this case is

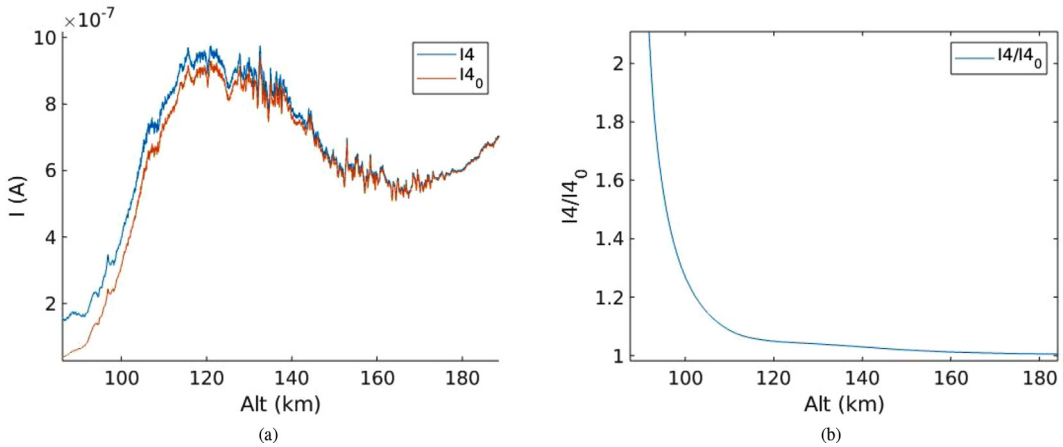

FIG. 5. (a) Real filtered current ($I4$) for ICI-4 sounding rocket, and its collisionally corrected ($I4_0$) current for the 4.5V biased probe. Figure (b) shows the ratio of real ($I4$) to corrected ($I4_0$) currents. Plots show only the relevant range of the upleg flight in the range 85–185 km. (Associated dataset available at https://doi.org/10.5281/zenodo.5647637) (Ref. 40).

down to ∼100 km from comparing Figs. 5(b) and 4(a). However, when a linear equation [exponent of γ_{corr} in Eq. (11)] does not hold, a nonlinear dependence on the collisional parameter λ_e/λ_D and possibly dimensionless probe voltage η seems to be present. A focused study on these effects is therefore important to perform in the future.

In addition, a function that includes the very highly collisional currents, where $\lambda_e/\lambda_D \lesssim 1$, is favorable. This area is of less practical interest, but it would nevertheless be instructive to include it in a generalized function. We would also like to do a study on the kinetic effects, i.e., how the electron distribution close to the probe changes in phase-space in the medium-to-high collisional range with respect to the collisionless case. We expect that there will be some differences, and that these will help to explain the mechanism of the enhanced collisional currents.

The results presented here should be relevant for any data analysis done on Langmuir probe currents from a collisional plasma in the electron saturation region. It is especially important to track the parameter λ_e/λ_D and know the limits of when collisionless theory is valid. This applies to both previous and future missions in the E-region, in addition to special cases like complex plasmas in a cometary tail or outgassing from a planet or moon, where neutral densities can be relatively high. It is our hope that this article will highlight the importance of a special treatment needed for such cases.

ACKNOWLEDGMENTS

This work received funding from the European Research Council (ERC) under the European Union's Horizon 2020 research and innovation program (Grant Agreement No. 866357, POLAR-4DSpace). This research is a part of the 4DSpace Strategic Research Initiative at the University of Oslo. This study is supported in part by the Research Council of Norway Grant No. 275653. T. Takahashi was supported by JSPS Overseas Research Fellowships and KAKENHI Grant No. JP20K14544.

We gratefully acknowledge Gullik Killie, Vigdis Holta, Trym Erik Nielsen, and Jan Deca, who took part in the development of PINC, along with Steffen Brask and Sigvald Marholm. We also wish to thank Richard Marchand, who provided PTetra for Sigvald Marholm to use.

We thank the staff of EISCAT for operating the facility and supplying the data. EISCAT is an international association supported by research organisations in China (CRIRP), Finland (SA), Japan (NIPR and ISEE), Norway (NFR), Sweden (VR), and the United Kingdom (UKRI). In this work, we used NRLMSISE-00, which was developed by Picone *et al.*[37] and is available at https://ccmc.gsfc.nasa.gov/modelweb/models/nrlmsise00.php.

AUTHOR DECLARATIONS

Conflict of Interest

The authors have no conflicts to disclose.

DATA AVAILABILITY

The data that support the findings of this study are openly available in Zenodo at http://doi.org/10.5281/zenodo.5906749, Ref. 39. The ICI-4 data are available in Zenodo at https://doi.org/10.5281/zenodo.5647637, Ref. 40. All simulations can be reproduced using PINC 0.2.0 available at https://github.com/pincproject.

REFERENCES

[1]A. I. Eriksson, R. Boström, R. Gill, L. Åhlén, S.-E. Jansson, J.-E. Wahlund, M. André, A. Mälkki, J. A. Holtet, B. Lybekk, A. Pedersen, L. G. Blomberg, and LAP Team, "RPC-LAP: The Rosetta Langmuir probe nstrument," Space Sci. Rev. **128**, 729–744 (2007).

[2]B. Holback, S. E. Jansson, L. Åhlén, G. Lundgren, L. Lyngdal, S. Powell, and A. Meyer, "The Freja wave and plasma density experiment," Space Sci. Rev. **70**, 577–592 (1994).

[3]G. Gustafsson, R. Boström, B. Holback, G. Holmgren, A. Lundgren, K. Stasiewicz, L. Åhlén, F. S. Mozer, D. Pankow, P. Harvey, P. Berg, R. Ulrich, A. Pedersen, R. Schmidt, A. Butler, A. W. C. Fransen, D. Klinge, M. Thomsen, C.-G. Fälthammar, P.-A. Lindqvist, S. Christenson, J. Holtet, B. Lybekk, T. A. Sten, P. Tanskanen, K. Lappalainen, and J. Wygant, "The electric field and wave experiment for the cluster mission," Space Sci. Rev. **79**, 137–156 (1997).

[4]K. S. Jacobsen, A. Pedersen, J. I. Moen, and T. A. Bekkeng, "A new Langmuir probe concept for rapid sampling of space plasma electron density," Meas. Sci. Technol. **21**, 085902 (2010).

[5]T. A. Bekkeng, K. S. Jacobsen, J. K. Bekkeng, A. Pedersen, T. Lindem, J.-P. Lebreton, and J. I. Moen, "Design of a multi-needle Langmuir probe system," Meas. Sci. Technol. **21**, 085903 (2010).

[6]H. Hoang, K. Røed, T. A. Bekkeng, J. I. Moen, A. Spicher, L. B. N. Clausen, W. J. Miloch, E. Trondsen, and A. Pedersen, "A study of data analysis techniques for the multi-needle Langmuir probe," Meas. Sci. Technol. **29**, 065906 (2018).

[7]H. Hoang, L. B. N. Clausen, K. Røed, T. A. Bekkeng, E. Trondsen, B. Lybekk, H. Strøm, D. M. Bang-Hauge, A. Pedersen, A. Spicher, and J. I. Moen, "The multi-needle Langmuir probe system on board NorSat-1," Space Sci. Rev. **214**, 75 (2018).

[8]H. M. Mott-Smith and I. Langmuir, "The theory of collectors in gaseous discharges," Phys. Rev. **28**, 727–763 (1926).

[9]G. Giono, N. Ivchenko, T. Sergienko, and U. Brändström, "Multi-point measurements of the plasma properties inside an Aurora from the SPIDER sounding rocket," J. Geophys. Res. **126**, e2021JA029204, https://doi.org/10.1029/2021JA029204 (2021).

[10]D. T. Farley, "The equatorial E-region and its plasma instabilities: A tutorial," Ann. Geophys. **27**, 1509–1520 (2009).

[11]M. M. Oppenheim and Y. S. Dimant, "Kinetic simulations of 3-D Farley-Buneman turbulence and anomalous electron heating," J. Geophys. Res. **118**, 1306–1318, https://doi.org/10.1002/jgra.50196 (2013).

[12]T. E. Sarris, E. R. Talaat, M. Palmroth, I. Dandouras, E. Armandillo, G. Kervalishvili, S. Buchert, S. Tourgaidis, D. M. Malaspina, A. N. Jaynes, N. Paschalidis, J. Sample, J. Halekas, E. Doornbos, V. Lappas, T. Moretto Jørgensen, C. Stolle, M. Clilverd, Q. Wu, I. Sandberg, P. Pirnaris, and A. Aikio, "Daedalus: A low-flying spacecraft for in situ exploration of the lower thermosphere-ionosphere," Geosci. Instrum., Methods Data Syst. **9**, 153–191 (2020).

[13]P. M. Kintner, B. M. Ledvina, and E. R. de Paula, "GPS and ionospheric scintillations," Space Weather **5**, 000260, https://doi.org/10.1029/2006SW000260 (2007).

[14]A. Gurevich, *Nonlinear Phenomena in the Ionosphere, Physics and Chemistry in Space* (Springer-Verlag, Berlin Heidelberg, 1978).

[15]Y. S. Dimant and M. M. Oppenheim, "Ion thermal effects on E-region instabilities: Linear theory," J. Atmos. Sol.-Terr. Phys. **66**, 1639–1654 (2004).

[16]M. Palmroth, M. Grandin, T. Sarris, E. Doornbos, S. Tourgaidis, A. Aikio, S. Buchert, M. A. Clilverd, I. Dandouras, R. Heelis, A. Hoffmann, N. Ivchenko, G. Kervalishvili, D. J. Knudsen, A. Kotova, H.-L. Liu, D. M. Malaspina, G. March, A. Marchaudon, O. Marghitu, T. Matsuo, W. J. Miloch, T. Moretto-Jørgensen, D. Mpaloukidis, N. Olsen, K. Papadakis, R. Pfaff, P. Pirnaris, C. Siemes, C. Stolle, J. Suni, J. van den IJssel, P. T. Verronen, P. Visser, and M. Yamauchi, "Lower-thermosphere-ionosphere (LTI) quantities: Current status of measuring techniques and models," Ann. Geophys. **39**, 189–237 (2021).

[17]F. Taccogna, S. Longo, and M. Capitelli, "Ion-neutral collision effects in Langmuir probe theory," Contrib. Plasma Phys. **48**, 509–514 (2008).

[18]Z. Zakrzewski and T. Kopiczynski, "Effect of collisions on positive ion collection by a cylindrical Langmuir probe," Plasma Phys. **16**, 1195–1198 (1974).

[19]G. Lapenta, "Particle simulations of space weather," J. Comput. Phys. **231**, 795–821 (2012).

[20]C. Cui and J. Wang, "Grid-based Vlasov simulation of collisionless plasma expansion," Phys. Plasmas **28**, 093510 (2021).
[21]C. Birdsall, "Particle-in-cell charged-particle simulations, plus Monte Carlo collisions with neutral atoms, PIC-MCC," IEEE Trans. Plasma Science **19**, 65–85 (1991).
[22]R. W. Hockney and J. W. Eastwood, *Computer Simulation Using Particles* (CRC Press, 1988).
[23]Y. Miyake and H. Usui, "New electromagnetic particle simulation code for the analysis of spacecraft-plasma interactions," Phys. Plasmas **16**, 062904 (2009).
[24]V. Vahedi and M. Surendra, "A Monte Carlo collision model for the particle-in-cell method: Applications to argon and oxygen discharges," Comput. Phys. Commun. Part. Simul. Methods **87**, 179–198 (1995).
[25]J. P. Verboncoeur, "Particle simulation of plasmas: Review and advances," Plasma Phys. Controlled Fusion **47**, A231–A260 (2005).
[26]H. Qin, S. Zhang, J. Xiao, J. Liu, Y. Sun, and W. M. Tang, "Why is Boris algorithm so good?," Phys. Plasmas **20**, 084503 (2013).
[27]M. M. Oppenheim and Y. S. Dimant, "Ion thermal effects on E-region instabilities: 2D kinetic simulations," J. Atmos. Sol.-Terr. Phys. **66**, 1655–1668 (2004).
[28]C. K. Birdsall and A. B. Langdon, *Plasma Physics via Computer Simulation* (McGraw-Hill, 1985).
[29]G. V. Killie, "A parallel multigrid Poisson solver for PINC, a new particle-in-cell model," Ph.D. thesis (University of Oslo, 2016).
[30]S. M. Brask, "Instabilities in collisional plasmas studied by means of 3D kinetic particle-in-cell simulations," Ph.D. thesis (University of Oslo, 2018).
[31]V. Holta, "Dynamics of a plasma blob studied with particle-in-cell simulations," Ph.D. thesis (University of Oslo, 2018).
[32]T. E. Nielsen, "Photoemissive charging of the mercury magnetospheric orbiter studied by means of 3D particle-in-cell simulations," Ph.D. thesis (University of Oslo, 2020).
[33]R. Marchand, "PTetra, a tool to simulate low orbit satellite-plasma interaction," IEEE Trans. Plasma Sci. **40**, 217–229 (2012).
[34]R. Marchand and P. A. Resendiz Lira, "Kinetic simulation of spacecraft-environment interaction," IEEE Trans. Plasma Sci. **45**, 535–554 (2017).
[35]S. Marholm and R. Marchand, "Finite-length effects on cylindrical Langmuir probes," Phys. Rev. Res. **2**, 023016 (2020).
[36]A. Brekke and J. Moen, "Observations of high latitude ionospheric conductances," J. Atmos. Terr. **55**, 1493–1512 (1993).
[37]J. M. Picone, A. E. Hedin, D. P. Drob, and A. C. Aikin, "NRLMSISE-00 empirical model of the atmosphere: Statistical comparisons and scientific issues," J. Geophys. Res. **107**, SIA 15-1–SIA 15-16, https://doi.org/10.1029/2002JA009430 (2002).
[38]D. Bilitza, "International reference ionosphere 2000," Radio Sci. **36**, 261–275, https://doi.org/10.1029/2000RS002432 (2001).
[39]S. M. Brask and S. Marholm (2021). "Ici-4 e-n collisional current simulations," Zenodo, V. 2.1, Dataset https://doi.org/10.5281/zenodo.5906749.
[40]A. Spicher, S. M. Brask, and W. J. Miloch (2021). "Multi-needle langmuir probe (mNLP) data on the investigation of Cusp irregularities (ICI) 4 sounding rocket," Zenodo, V. 2.1, Dataset https://doi.org/10.5281/zenodo.5647637.